Fire activity in the northern Arctic tundra now exceeds late Holocene levels, driven by increasing dryness and shrub expansion

5 Angelica Feurdean^{1,2*}, Randy Fullweber, Andrei-Cosmin Diaconu⁴, Graeme T. Swindles^{5,6} Mariusz Gałka*⁷

¹Institute of Physical Geography, Goethe University, Altenhöferallee 1, 60438, Frankfurt am Main, Germany

²STAR-UBB Institute, Babeș-Bolyai University, Kogălniceanu 1, 400084, Cluj-Napoca, Romania

³Toolik Field Station, Institute of Arctic Biology, University of Alaska Fairbanks, 2120 N. Koyukuk Drive, AK 99775-7005,

10 Fairbanks, United States of America

20

25

⁴Department of Geology, Babes-Bolyai University, Kogălniceanu 1, 400084, Cluj-Napoca, Romania

⁵School of Natural and Built Environment, Queen's University, H3P6+29C, Belfast, UK

⁶Ottawa-Carleton Geoscience Centre and Department of Earth Sciences, Carleton University, Ottawa, Canada

⁷Faculty of Biology and Environmental Protection, Department of Biogeography, Paleoecology and Nature Conservation,

University of Lodz, Banacha 1/3, 90-237 Lodz, Poland

Correspondence to: Angelica Feurdean (feurdean@em.uni-frankfurt.de) and Mariusz Gałka (mariusz.galka@biol.uni.lodz.pl)

30 Abstract

Tundra ecosystems are characterized by small, rare and infrequent fires due to cold, often waterlogged conditions, and limited biomass. However, ongoing climate warming and drying in northern soils and peatlands are contributing to increasingly frequent and extensive wildfires. To place recent fire regimes in the context of long-term variability and to better understand interactions between fire, moisture and vegetation, we reconstructed wildfire history over the past 3000 years using a network of charcoal records in combination with vegetation and hydrological datasets and satellite-derived fire datasets from in northern Arctic Alaska peatlands. The composite charcoal record shows minimal fire activity from ~1000 BCE to 1000 CE, followed by a modest increase between 1000 and 1200 CE, and then a renewed decline. This long-term pattern shifted abruptly after 1900 CE, reaching its maximum between 1950 and 2015 CE, when fire activity exceeded any levels observed in the preceding three millennia. Individual charcoal records show a spatially heterogeneous pattern in fire occurrence before 1950 CE, and a 40 more homogeneous one thereafter. Our findings suggest that the deepening of water tables and peatland drying associated with permafrost thaw have facilitated woody encroachment, especially by more flammable Ericaceous shrubs. These vegetation changes have increased fuel availability and flammability, ultimately driving the recent surge in wildfire activity and highlighting the growing vulnerability of Arctic tundra ecosystems to fire. We also found that the charcoal source area of our tundra fire encompasses broader landscapes over tens of kilometre. Our study emphasizes the significance of long-term, multidisciplinary research in documenting moisture-vegetation-fire feedbacks that influence tundra fire regimes. Ultimately, this long-term fire dynamic study provides critical context for evaluating recent changes and incorporating tundra peatland fire risk into global climate mitigation strategies.

1 Introduction

Short-term records of fire activity derived from satellite observations indicate that many northern tundra regions have experienced an unprecedented increase in the number, size, and intensity of individual fires, as well as the length of the fire seasons in recent decades (Descals et al., 2020; Scholten et al., 2021, 2024). The Arctic tundra biome inhabits some of Earth's coldest regions, characterized by low above-ground biomass productivity. However, Arctic regions store approximately half of the global belowground soil organic carbon in peatlands (Loisel et al., 2021). Cold and waterlogged conditions in Arctic soils and peatlands often constrain fires to small, rare, and infrequent events, limiting burning depth and carbon loss (Archibald et al., 2013; Turetski et al., 2015; Whitman et al., 2018, 2019; Sayedi et al., 2024). Recent rising temperatures, increased lightning frequency, changes in peatland hydrology, and greater shrub biomass contributed to a deviation from the previously low fire activity (Scholten et al., 2024). Well-hydrated peatlands composed of moss and sedges can be resistant to droughts and exhibit only moderate surface fire damage compared to peatlands dominated by shrub and tree communities (Magnan et al., 2012; Kettridge et al., 2014; Whitman et al., 2018). Deep burns can smoulder over winter in hydrologically disturbed peatlands and re-ignite during spring (Scholten et al., 2021).

While satellite data offer high temporal and spatial resolution of many aspects of the fire regime, they are limited to the past few decades. Therefore, satellite records alone cannot reveal how recent aspects of fire regimes compare to longer-term

variability. Charcoal analysis from sedimentary records provides critical insights into the long-term dynamics of fire, offering essential spatial-temporal context for assessing recent changes. Combined with reconstructions of vegetation communities and hydrological conditions, enables the investigation of past tundra fire regimes under various climatic conditions and vegetation compositions (Higuera et al., 2018; Vachula, 2020; Hoecker et al., 2020; Sim et al., 2023). Therefore, approaches with a broad temporal and spatial scope enable an evaluation of feedbacks between fire and drivers, forming a foundation for understanding how tundra fire regimes may respond to future climate and vegetation development scenarios.

Although some palaeoecological records of tundra fires in Arctic Alaska exist, mainly from lake archives (Hu et al., 2010; Higuera et al., 2008; Chipman et al., 2015; Chipman and Hu, 2017; Vachula, 2020; Hoecker et al., 2020; Chipman et al., 2025; Fran-DePue and Chipman, 2025), combined records documenting fire history, plant species composition, and hydrological variability from peatlands remain rare (Gałka et al., 2018; Cleary et al., 2024). The lack of a multiproxy approach limits our understanding of how fires interact with vegetation and hydrological conditions. Another challenge in reconstructing past tundra fires is understanding the source areas of charcoal and the amount of charcoal incorporated into fossil records during fire events (Vachula et al., 2020). Compared to lakes, peatlands provide local-scale reconstructions of past fire regimes, with the source area of charcoal from a fire typically extending only a few kilometres (Conedera et al., 2009; Remy et al., 2018). This fine-scale resolution reflects the pronounced heterogeneity in local peat moisture, vegetation composition and structure, and the relatively small catchment area (Magnan et al., 2012; Remy et al., 2018; Barhoumi et al., 2019; Stivrins et al., 2019; Feurdean et al., 2020; Kuosmanen et al., 2023). Because wildfire patterns are highly variable at a small spatial scale, multisite peatland reconstructions are necessary to identify broader trends in fire regime dynamics beyond the local scale.

To place modern fire regimes in the context of long-term variability, we reconstructed 3,000 years of wildfire history using six new and three previously published macrocharcoal records from a tundra region north of the Brooks Range in Arctic Alaska. We combined satellite and charcoal records, primarily from the tussock and shrubby tussock tundra zones, with data on local (plant macrofossils) and regional (pollen) vegetation and hydrological changes (testate amoebae) to investigate how interactions between peatland hydrology and vegetation affect fuel availability, dryness, and flammability. We hypothesize that the recent increase in fire frequency in northern Alaska is linked to the lowering of the permafrost layer and the deepening of the water table, resulting in the expansion of shrubs on dry peatlands. We also aim to refine the understanding of charcoal source areas in tundra fire reconstructions by comparing our charcoal records with satellite-derived data on fire size and frequency.

2. Geographical location and sites selection

85

90

The study area is located within the continuous permafrost zone of northern Alaska, on the northern side of the Brooks Range Mountains (Fig. 1). The landscape features a mosaic of peatland types, small glacial lakes, kames, and moraines (Hamilton, 1986). The region experiences a continental Arctic climate, with a mean annual temperature of approximately 0°C. Mean seasonal temperatures range from –22.5 °C in winter to +11.2 °C in summer. Annual precipitation averages 250 mm, falling predominantly as snow (Environmental Data Center Team, 2017). The number of snow-free days is approximately 110,

although brief snowfall can occur during summer (Cox et al., 2017; https://akclimate.org/data/annual-reports). The main vegetation types are dwarf-shrub and tussock sedges-moss-dwarf shrub communities, composed of sedges, brown mosses, *Sphagnum*, and shrub species, with composition varying by site (Walker et al., 1994, 2005; Table 1; Appendix A).

The study sites were distributed along a 150 km transect parallel to the Dalton Highway, extending from the northern foothills of the Brooks Range to the Arctic Ocean (Fig. 1). In the summer of 2015, we collected nine cores from six peatlands and one dry up hollow. Peat cores (monoliths) were retrieved using a long-bladed shovel, dug to the mineral substrate, and the sediments from the hollow were retrieved using a Russian-type corer. All cores were placed in PVC tubes, transported, and deposited in a cold room at the University of Łódź, Poland (Gałka et al., 2018). Details on geographic coordinates, elevation, core lengths, and dominant vegetation at the coring points are provided in Table 1.

3 Material and methods

3.1 Chronology

100

105

115

120

125

130

Chronologies were established using radiocarbon dating via Accelerator Mass Spectrometry (AMS), applied to a combination of plant macrofossils and bulk peat samples, supplemented by ²¹⁰Pb dating for recent sediments (Table B1). Detailed chronology for Toolik I and II (TFSI and II) are published in Gałka et al. (2018), for GaI and GaII in Gałka et al. (2023), and for NBb and Erin are presented in Gałka et al. (2025). Age-depths models for all sites are presented in Appendix B, along with details on chronology for the three unpublished sites, SG, RH, and DL.

3.2 Macroscopic charcoal inferred fire history

We reconstructed changes in local-scale fire activity based on macroscopic charcoal analysis of 1–2 cm³ sample volumes taken at 1 cm contiguous intervals across cores from all sites. Sample preparation involved overnight bleaching using sodium hypochlorite (domestic bleach) and wet sieving through a 150 µm mesh. Charcoal identification and categorization of morphotypes (the latter conducted for six of the eight records) followed the protocols of Feurdean et al. (2017) and Feurdean (2021). Charcoal morphologies were then grouped into non-woody (graminoids and forbs) and woody to determine the dominant fuel type. We also separate the charcoal fractions (5 out of 8 records) into two size classes: 150–500 µm and >500 µm, to distinguish more local from more regional fires (Adolf et al., 2018). Additionally, we searched for large macrocharcoal fragments in samples used for plant macrofossil analysis. For this, 12 cm³ contiguous sediment samples were washed and sieved using a 200 µm mesh without applying bleaching, following Gałka et al. (2018).

Charcoal accumulation rate (CHAR particles cm² yr⁻¹) was calculated by dividing the particle concentration (particles cm³) by the deposition time derived from the age-depth models (yr cm⁻¹). To account for changes in sedimentation rates, which increased markedly in the upper sections of the records, CHAR values were interpolated to a median temporal resolution for each record.

3.3 Plant macrofossils and pollen-based reconstruction of vegetation dynamics

We extracted shrub abundance from existing plant macrofossil and pollen records from TFSI, TFSII (Gałka et al. (2018), GaI, GaII (Gałka et al. (2023)), NBb, and Erin (Gałka et al. (2025) to determine the local and regional changes in woody vegetation (Table 1). Total shrub pollen percentages represent the combined abundance of *Betula nana*, *Alnus*, *Salix*, Ericaceae, *Vaccinium*, *Rubus chamaemorus*, and *Dryas octopetala*. For plant macrofossils, above-ground remains (seeds, leaves, and fruits) of *Andromeda polifolia*, *Betula nana*, *Ledum groenlandicum*, *Vaccinium*, and *Salix* spp. were quantified as counts. In contrast, the abundance of unidentified shrub roots was expressed as a volume percentage relative to the total vascular plant and moss remains.

140 3.4 Testate amoebae reconstruction of hydrological changes

145

150

155

160

165

Changes in peatland hydrology were assessed using existing testate amoeba-based water table depth (DTW) reconstructions from the TFSI, TFSII (Taylor et al., 2019), GaI, GaII (Gałka et al., 2023), and Erin (Gałka et al., 2025). All cores were collected from similar peatland types, specifically small hummock microforms. Quantitative reconstructions of water table depth were derived using the transfer function developed by Taylor et al. (2019).

3.5 Composite records of fire, vegetation, and hydrological changes

To assess fire history across the study area, we developed a composite record of charcoal accumulation rate by combining all individual interpolated charcoal records (n = 9). We generated a composite CHAR record following the protocol of Blarquez et al. (2014), which involves MinMax re-scaling, a Box–Cox transformation to homogenize variance across records, and Z-score standardization using a baseline period of 2 ka. The transformed time series was smoothed using a LOWESS smoother with a 200-year window. Confidence intervals were estimated from the distribution of 1,000 bootstrapped replicates.

To determine local and regional changes in woody vegetation, we created composite records of shrub abundance derived from individual pollen and plant macrofossil datasets (n = 5). For plant macrofossils, two separate composite records were constructed, one for above-ground remains (seeds, leaves, and fruits) and one for root remains. Composite pollen and macrofossil time series were generated by binning in 50-year steps and applying a LOWESS smoothing with a 200-year window.

Hydrological changes were reconstructed by creating a composite testate amoeba-based water table record (n=5). This was developed by combining existing individual records of depth-to-water table (DTW) reconstructions, using a Z-score transforming the DTW data (Swindel et al., 2019), and applying a LOWESS smoothing with a 200-year window.

3.4 Fire identification from satellite images

To determine recent trends in fire activity, evaluate our understanding of charcoal source areas, and the amount of charcoal produced in tundra fire, we downloaded two datasets available from the Alaska Interagency Coordination Center (AICC) website: Alaska Fire History Location Points (fire points) and Alaska Fire History Perimeter Polygons (fire polygons) (Miller et al., 2023). In case of fire polygons, the area burned was based on the size of the polygon; non-vegetated surfaces were not

removed. In case of fire point data, the reported incident size was estimated from field observations or calculated using GIS from perimeter polygons; therefore, the recovered size of fire from fire point data should be treated with caution. Spatial analysis was conducted using ArcGIS v. 3.4.3 with the coordinate system set to the Alaska Albers Equal Area Conic (EPSG: 3338) projection. We identified those fire points (n=35) and fire polygons (n=9) that fell within 2, 25, and 70 km from the Dalton Highway, north of the Brooks Range (Fig. 1). We calculated the distance from each fire point and fire polygon from the Dalton Highway as well as the distance from the nearest five fire points to each of the fossil record. For the fire point data, an estimate of the area burned is provided in hectares. For the polygon data, the size of the fire is reported as area in hectares, determined by the ArcGIS' Calculate Geometry Attributes tool (S1).

175 **4. Results**

180

185

190

195

4.1 Charcoal based biomass burning

Of the nine macrocharcoal records analysed, seven span the last one to two millennia, while only two extend as far back as 1000 BCE albeit at low temporal resolution (Fig. 2). CHAR values are consistently low across all sites, ranging from 0 to 1.07 particles cm⁻² yr⁻¹ (mean = 0.04 ± 0.11). The highest mean CHAR values were observed at SG (0.05 particles cm² yr¹) and NBb (0.09 particles cm² yr¹). Interpolated individual and composite CHAR records indicate consistently low biomass burning (negative Z-scores) between ~1000 BCE and 1000 CE (Fig. 3). A temporary increase in composite CHAR is observed after ~1000 CE, peaking around 1200 CE (positive Z-scores), followed by a decline to negative Z-scores; however, values remained higher than those recorded prior to 1000 CE. Elevated CHAR values around 1200 CE are particularly visible at TFSII, NBb, ER and RH. A continuous rise in composite CHAR begins around 1900 CE, reaching its maximum between 1950 and 2015 CE (positive Z-scores), a trend consistently reflected across all individual records.

The charcoal morphological record indicates an almost equal representation of herbaceous (e.g., grass leaves and stems of grasses and forbs) and woody charcoal morphologies, with higher woody influx towards recent times (Fig. 2). Small-size charcoal particles (150–500 µm) dominate over the larger fraction (>500 µm) (Appendix C). No large macrocharcoal fragments (>1 mm) were detected in plant macrofossil records.

4.2 Satellite and charcoal-based fire record: a comparison

Our satellite imagery record of fire points within a 70 km buffer along the Dalton Highway shows that 36 fires occurred between 1969 and 2023. Except for an extremely large fire of 103896 ha occurring in 2007, most recorded fires were of small size (mean = 46 ha; median = 2 ha). Fire polygon data indicate nine fires with a mean size of 11825 ha (median = 115 ha; Figs. 1a, 4a; S1). There were 10 recorded fires (0.5 per year) between 1969 and 1990, followed by a fire-free period from 1990 to 2001 (Fig. 4ab). Fire activity increased markedly between 2001 and 2017, with 23 recorded fires (1.5 per year), before declining again, with only one fire observed in 2023.

On a temporal scale, we found that the nearest fires to the sampling points (range 3-29 km; mean 12 km) occurred in years 1971, 1979, 1990, and 2007, and the nearest sampling points to these fires were TFSII (3 km), DL (6.5 km), and RH (7 km)

(Figs. 1a,b, 4b; S1). The second closest fires from the charcoal sampling (range 15-31 km; mean 20 km) occurred in years 1969, 1970, 1971, 1979, 1983, 1990, 2004, 2007, 2017 (S1). Given the inherent chronological uncertainties in sedimentary records and the very low amount of charcoal in our data, the slight increases in interpolated CHAR centred around the years 1965-1975, 1985-1990, and 2010-2015, may correspond to documented fire events occurring during seasons 1969–1983, 1990 and 2004-2017 (Figs. 1a,b, 4a; S1). However, the CHAR record suggests greater burning activity around the 1970s. In contrast, satellite data indicate maximum fire size and frequency between 2001 and 2017 CE (Fig. 4a).

4.3 Vegetation changes

210

215

220

230

The pollen-based composite vegetation record, representing shrub abundance at local to regional scales, indicates consistently low shrub abundance (~12%) between 1000 BCE and 500 CE (Fig. 3b). A slight increase is observed from 250 CE (~15%) and again between 500 and 1000 CE (~20%). A marked rise in shrub abundance (~40%) occurs from approximately 1400 CE to the present, interrupted by brief declines between 1800 and 1945 CE and in the most recent samples.

The composite plant macrofossil record, reflecting local-scale shrub abundance, shows very low percentages of above-ground remains (~2%) from 1000 BCE to 1950 CE (Fig. 3b). A sharp increase (~15%) occurs after 1950 CE, continuing to the present. In contrast, the below-ground macrofossil record (roots) shows an increase beginning around 1900 CE, and after 1950 CE. A slightly elevated root abundance is also evident between ~750 and 250 BCE (Fig. 3b).

4.4 Hydrological changes

The composite water table record indicates predominantly low (deep) water levels (positive Z-scores) between ~250 and 500 CE and again between ~1250 and 1600 CE, with persistently low levels over the past ~50 years (Fig. 3d). The pronounced deepening around 250 CE is primarily driven by lower water levels at two of the three available sites: TFSII (Taylor et al., 2019) and NBb (Gałka et al., 2025). In contrast, shallow water levels (negative Z-scores) are primarily recorded between ~500 and 1250 CE.

5. Discussion

225 5.1 Charcoal source areas in tundra fire reconstructions

Our analysis of charcoal size classes reveals that most particles fall within the 150–500 µm range, with only a small proportion exceeding 500 µm, and no macrocharcoal fragments (>1 mm) are identified (Fig. 2; Appendix C). The dominance of smaller particles, together with evidence that the nearest recent fires occurred at a mean distance of ~12 km away, suggests that the charcoal source areas of our tundra fires encompass broader landscapes (Figs. 1, 4c). Whilst typical source areas for macrocharcoal are estimated to be a few kilometers, particularly in peatlands, regional source areas extending to 20 kilometres and beyond, i.e., up to 100 kilometres, have also been reported (Higuera et al., 2005, 2007; Adolf et al., 2018; Vachula et al., 2020). This is particularly true for smaller, lighter, and more aerodynamic particles, often of herbaceous origin, or under the specific wind and fire behaviour conditions (Vachula et al., 2020; Vachula & Rehn, 2023).

The timing of elevated charcoal accumulation rates in isolated but mostly in several consecutive samples around 1965-1975, 1985-1990, 2005, and 2010-2015, corresponds reasonably well with periods of frequent fires documented by satellite records (Figs. 1a,b, 4a). The high CHAR values observed in 2005 and between 2010 and 2015 (Fig. 4a), particularly at sites 1 to 7 (Fig. 2), may have been derived from the large fires, such as the Anaktuvuk River fire (2007), and others that occurred in 2007 (Fig. 1a,b), suggesting a link with fire size. The occurrence of a few small fires is also noted in 2000s (white dots) and 2010s (yellow dots; Fig. 1b) near most sites. In contrast, the elevated CHAR values in the 1970s (Fig. 4a), particularly evident at sites 5 to 9 (Fig. 2), correspond to a few small fires near these sites (Fig. 1b, pink dots), implying a link to the proximity of fire. However, because the closest documented fires occurred at considerable distances (3–29 km) from our sampling sites, and fire source areas often overlapped, it remains difficult to conclude whether the elevated CHAR values primarily reflect fire size and proximity, or a combination of both.

An intriguing outcome of the charcoal–satellite comparison is that the most recent large fires (2001–2015 CE) are associated with lower-amplitude charcoal signals. This feature contrasts with the occurrence of less frequent, smaller fires between 1969 and 1985 CE and higher charcoal levels (Fig. 4). This discrepancy may relate to differences in the amount and type of biomass burned. Graminoids produce substantially less charred material per unit biomass than forbs and shrubs, particularly ericaceous species. High fire temperatures can lead to near-complete biomass consumption, resulting in the production of ash (Pereboom et al., 2020; Feurdean et al., 2021). Peatland dryness has intensified in recent times, potentially favouring higher fire temperatures and complete biomass combustion and may therefore explain the low charcoal values observed during recent large fires. These findings highlight the complexity of interpreting charcoal records, as charcoal abundance reflects not only fire size and proximity, but also fuel amount and type, as well as combustion conditions (see Section 5.3).

5.2 Pattern in Arctic Alaska peatland burning

- Our satellite-based fire database from the northern slopes of the Brooks Range along the Dalton Highway agrees with previous findings that many tundra ecoregions of Alaska have experienced a marked increase in fire frequency and size over the past five decades (Higuera et al., 2008; Vachula, 2020; Scholten et al., 2024; Miller et al., 2023). Specifically, our data show that lightning-ignited fires occurred at an average rate of 0.5 per year between 1969 and 1990, followed by a fire-free period from 1990 to 2001 CE. Fire activity surged again between 2001 and 2017 CE, with an average of one fire every 1.5 years and larger burned areas, before declining in the most recent years (Fig. 4a,b). Historical evidence from 1948 aerial imagery further documents tundra fires that burned sometime between 1880 and 1920 on the northern Brooks Range, i.e, near the Ketik and Meade Rivers, Shivugak, and Starfish Bluff, with additional anecdotal records mentioning fires in 1952 and 1959 on the Arctic Slope (Miller et al., 2023).
- Our individual and composite charcoal records spanning the past three millennia indicate very low fire activity in Arctic tundra from ~1000 BCE to 1000 CE (Figs. 2, 3). A slight increase occurred after 1000 CE, peaking around 1200 CE, but overall burning remained low until ~1950 CE, when both individual and composite records show an abrupt and unprecedented rise in fire activity. This recent increase contrasts sharply with the rare and long fire-free intervals of the Holocene and supports

findings from other tundra ecoregions in Arctic Alaska in documenting unusually frequent fires in these cold, with low-above ground biomass ecosystems (Higuera et al., 2008, 2011; Chipman et al., 2015; Hu et al., 2015; Vachula, 2020; Hoecker et al., 2020; Fran-DePue and Chipman, 2025). Holocene charcoal records from the northern slope of Alaska further indicate that fire return intervals were even longer prior to 3000 years ago. However, shorter fire cycles, like those observed in modern tundra fires, were also detected (Fran-DePue and Chipman, 2025). Another finding of our study is that individual charcoal records show a heterogeneous pattern in fire occurrence before 1950 CE, and a more homogeneous one thereafter, consistent with the emergence of more regularly occurring fires in recent decades. Lower temporal resolution and larger age control errors in the older part of the sediments could have also contributed to this apparent heterogeneity. However, the more elevated values in biomass burning around 1200 and 1600 CE, visible at multiple sites, suggests that homogenous fire occurrence across sites in the distant past could also be reconstructed.

5.3. Drivers of peatland burning

300

280 Recent increases in temperature and lightning frequency are often cited as key drivers of enhanced fire activity across Arctic tundra regions (Hu et al., 2010, 2015; Hoecker et al., 2020; Sim et. al., 2023; Scholten et al., 2024). Our independent reconstruction of peatland hydrology reveals that the lowest water table levels (positive Z-score), indicating the driest conditions of the late Holocene, occurred in the past few decades, coinciding with an intense fire period (Fig. 3). This recent deepening of water table was attributed to warming-induced permafrost thaw (Taylor et al., 2019; Gałka et al., 2023; Cleary 285 et al., 2024). Nevertheless, we identified two earlier episodes of lowered water tables: a pronounced drying between ~250 and 500 CE and a lower amplitude drying between ~1250 and 1600 CE (Fig. 3). The ~250-500 CE dry period was primarily determined by low water levels at TFSII (Taylor et al., 2019) and NBb (Gałka et al., 2025), but only TFSII shows a corresponding increase in charcoal accumulation rates (Figs. 2, 3), suggesting that peatland drying did not consistently translate into higher fire activity during this period. In contrast, the ~1250–1600 CE dry period coincides with greater but overall 290 pronounced fluctuations in composite biomass burning, however, peak biomass burning occurs between 1000-1200 CE, thus before the onset of water level deepening. Arctic Alaska experienced cooler temperatures and decreased moisture during the late Holocene (Taylor et al., 2019; Fran-DePue and Chipman, 2025) as well as higher fire activity (Fran-DePue and Chipman, 2025). The reduced summer precipitation and lower temperatures of the Little Ice Age (~1250–1600 CE) are documented to have deepened the peatland water tables (Taylor et al., 2019; Zhang et al., 2022). Drier peatland conditions likely promote the 295 desiccation of surface fuels, increasing their flammability and likelihood of ignition and sustained burning (Katrigge et al., 2020; Feurdean et al., 2022).

Our multiproxy palaeorecords provide a unique opportunity also to examine local feedbacks between fuel type and availability, as well as fire, particularly in areas prone to pronounced drying, such as hummocks. Plant macrofossil data show the highest abundance and diversity of shrub communities, *Betula nana*, undifferentiated Ericaceae, *Ledum*, *Andromeda*, *Vaccinium*, and *Salix*, after 1900 CE, with a notable increase after 1950 CE (Fig. 3). The pollen record, reflecting landscape-scale vegetation composition, shows a pattern of shrub expansion around 500–700 CE, 1200–1600 CE, and after 1950 CE; Fig. 3). Thus,

similarly to biomass burning, shrub abundance (particularly shrubs pollen) has generally increased over the last millennium and peaked in recent decades, and this increased largely preceded that of biomass burning. The visual correlation between increased fire activity and expanded shrub cover suggests that greater woody biomass, thus fuel quantity promoted enhanced fire. Although this relationship could not be confirmed statistically (not shown), our results suggest a complex role for moisture–vegetation feedbacks in shaping fire regimes in Arctic tundra ecosystems.

Pollen and macrofossil evidence also indicate a compositional change in the shrub and their behaviour to fire, that may have affected the fire-vegetation relationship. There is a shift from *Alnus* and *Salix*, which were dominant before 1850 CE, to an increased abundance of Ericaceous shrubs and, to a lesser extent, *Betula nana* in recent decades (Gałka et al., 2018, 2023, 2025). *Salix* and *Alnus* typically grow on dry mineral soils, whereas Ericaceous shrubs are characteristic of peaty soils, which have become drier in recent decades. Ericaceous shrubs are also highly flammable and re-establish post-fire, while *Betula* species resprout vigorously following fire (de Groot et al., 1999, 2013). A strong link between the expansion of resprouting taxa, such as *Betula glandulosa*, and elevated fire activity has been documented in north-central Alaska during the Lateglacial and early Holocene periods (Higuera et al., 2008). The satellite-derived vegetation maps reveals that the many recent fires in the study area occurred in tussock sedge—dwarf shrub and dwarf shrub communities (Appendix A).

Finally, temporal mismatches among our fire, vegetation, and moisture records could be attributed to taphonomic processes. Plant assemblages were dominated by graminoids (Cyperaceae) and mosses, primarily *Sphagnum*, with shrubs becoming abundant only in the past ~500 years (pollen record) and especially over the past decades (plant macrofossils). Because graminoids and mosses produce little charcoal per unit biomass and combust rapidly (Pereboom et al., 2020; Feurdean et al., 2021), low charcoal accumulation during earlier dry periods may also reflect this herbaceous—moss dominance. Further, differences in the temporal and spatial resolution of proxies and speed of ecosystem responses may have contributed to temporal offsets among them. Pollen and macrocharcoal (especially particles <500 µm) integrate regional to local vegetation and fire signals, whereas plant macrofossils and testate amoebae primarily reflect local and extra-local peatland conditions. Consistent with these differences, pollen-inferred shrub expansion appears to show a better temporal correspondence with increased charcoal-inferred biomass burning than do plant macrofossils or water-table reconstructions.

Conclusion

Our research presents the first comprehensive synthesis of charcoal data from northern Alaska peatlands, integrating local and regional records of vegetation and hydrological change to investigate how interactions between peatland hydrology and vegetation influence fuel availability, flammability, and fire occurrence. The composite charcoal record reveals minimal fire activity from ~1000 BCE to 500 CE, followed by a slight increase thereafter. After 1950 CE, fire activity surpassed all levels observed over the previous three millennia. While individual charcoal records indicate a heterogeneous pattern in fire occurrence prior to 1950 CE, more recent decades show a transition to increasing homogeneity, reflecting the feature of more commonly occurring fires in recent decades. Our study also emphasizes the importance of multidisciplinary research in documenting moisture–vegetation–fire feedbacks that shape tundra fire regimes, with implications for ongoing Arctic greening

and warming. By offering new insights into long-term and broad-scale burning activity in this region, it also emphasizes the importance of incorporating tundra peatland fire regimes into mitigation strategies for global high-latitude regions.

Appendices:

340 **Appendix A.** The dominant vegetation type in the study region.

Appendix B. Chronology.

Appendix C. Charcoal influx of particles larger then $> 500 \mu m$.

Data availability: The datasets were sent to Neotoma.

Supplement S1 Satellite-based information of fire names, coordinates, size, and distance from the Dalton Highway and charcoal sampling sites.

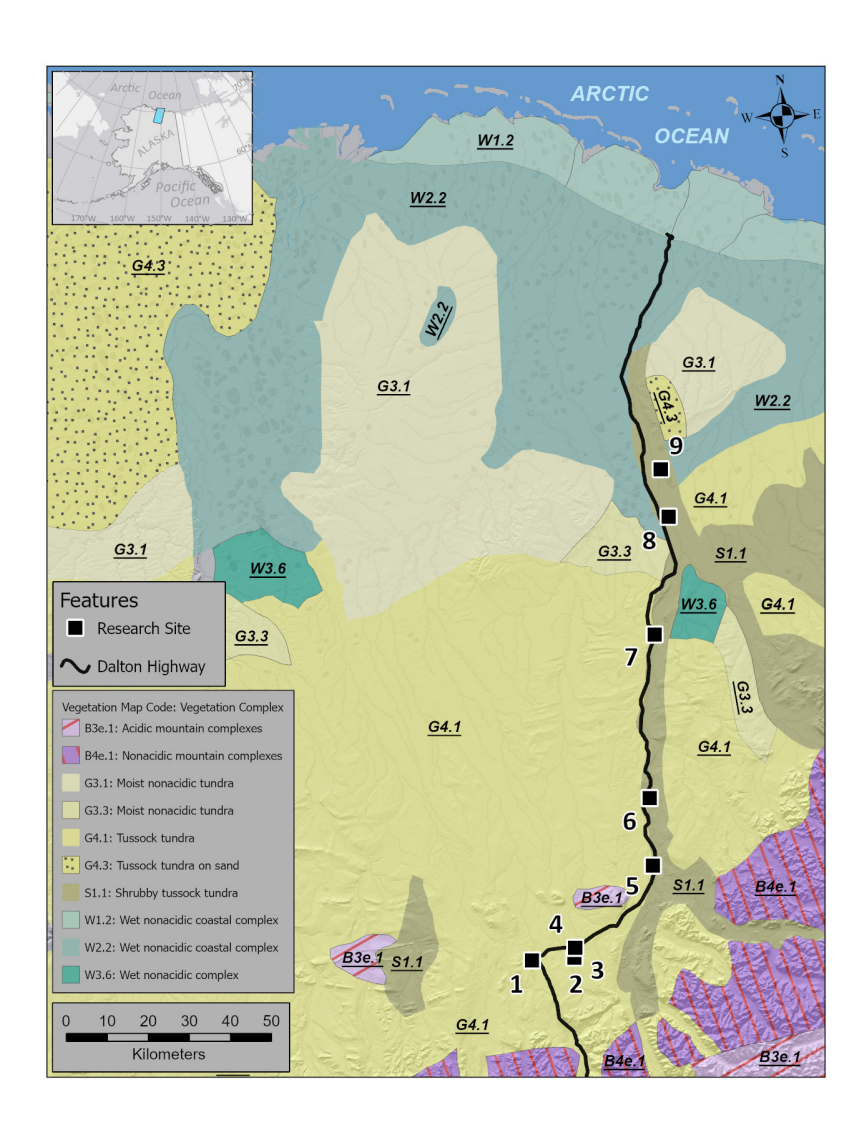
Author contribution: AF and MG conceived study. AF, ACD, RF, GS, MG, performed the analysis. AF prepared the manuscript with contributions from MG. All authors contributed to review and editing.

Competing interests: The authors declare that they have no conflict of interest.

Acknowledgements: We thank Liam Taylor for performing the testate amoeba analysis at TFS I and II.

Financial support: The research has received support from National Science Centre (Poland) grant No UMO-2019/35/B/ST10/00367 (PI: Mariusz Gałka). AF acknowledges support Deutsche Forschungsgemeinschaft (grant no FE_1096/9) during writing stage

Appendix Fig. A1 The dominant vegetation type in the study region which depicts the main vegetation types where historical fires occurred. For details, see Fig. 1.



Appendix B. Chronology

360

The AMS radiocarbon measurements at all sites are presented in Table B1a. The calibration of the radiocarbon dates and the construction of the age depth models were taken from the original publications and were performed with OxCal 4.4.4 software (Bronk Ramsey, 2009) and the IntCal13 (Reimer et al., 2013) or IntCa20 (Reimer et al., 2013, 2020) and post-bomb NH1 (Hua et al., 2022) calibration curves (visible in each figure insert). The Bayesian age-depth models were calculated by applying the $P_Sequence$ function (parameters = 1 cm-1, log10(k/k0) = 1 and interpolation = 0.5 cm). BCE before Common Era. CE Common Era.

Table B1a AMS ¹⁴C measurements at nine investigated sites. pMC =denote modern ¹⁴C, post 1950 CE

Site / Depth (cm)	Material dated	Lab. Code	¹⁴ C dated	
TFSI 18-19	Sphagnum stems	Poz-79187	$150.28 \pm 0.67 \text{ pMC}$	
TFSI 23-24	10 fruits of <i>Carex</i> sp.	Poz-80735	195 ± 30 BP	
TFSI 35-36	3 fruits of <i>Carex</i> sp., wood	Poz-80733	930 ± 30 BP	
TFSI 43-44	4 leaves of Andromeda polifolia	Poz-79188	1255 ± 35 BP	
TFSII 13-14	Leaf of Betula nana, Pleurozium schreberii remains	Poz-80729	$109.21 \pm 0.35 \text{ pMC}$	
TFSII 19-20	Wood, Sphagnum stems	Poz-80730	$325 \pm 30 \text{ BP}$	
TFSII 29-30	Leaf of Betula nana	Poz-79189	990 ± 40 BP	
TFSII 39-40	Sphagnum leaves	Poz-80731	$1610 \pm 60 \text{ BP}$	
TFSII 48-49*	bulk peat	Poz-80732	950 ± 30 BP	
GaI 8.75	Sphagnum stems	Poz-135852	$125.8 \pm 0.49 \text{ pMC}$	
GaI 16.75	Sphagnum stems	Poz-135853	$134.3 \pm 0.4 \text{ pMC}$	
GaI 24.75	Sphagnum stems	Poz-136575	$100 \pm 30 \text{ BP}$	
GaI 31.75	Sphagnum stems	Poz-136576	295 ± 30 BP	
GaI 37.75	Sphagnum stems, Salix leaf	Poz-136577	270 ± 30 BP	
GaI 42.5	Sphagnum stems	Poz-108708	415 ± 30 BP	
GaII 7.75	Aulacomnium palustre stems with leaves, Polytriastrum alpinum stems with leaves	Poz-135797	$105.8 \pm 0.34 \text{ pMC}$	
GaII 16.75	Polytrichaceae stems	Poz-136578	$107.51 \pm 0.35 \text{ pMC}$	
GaII 23.75	Sphagnum stems and branches	Poz-136579	230 ± 30 BP	
GaII 34.75	Sphagnum stems, Straminergon stramineum stems with leaves, leaf's fragm.		280 ± 30 BP	
GaII 40.75	Sphagnum stems Poz-135798		$350 \pm 30 \text{ BP}$	
Ga 47.5	Sphagnum stems Poz-108710		545 ± 30 BP	
NBb 13.25	Sphagnum stems, Betula nana leaves Poz-		$125.8 \pm 0.49 \text{ pMC}$	
NBb 20.75	Sphagnum stems	Poz-135145	130 ± 30 BP	
NBb 26.75	Wood pieces	Poz-135146	280 ± 30 BP	
NBb 39.75	Carex fruits x10 and Scorpidium scorpioides leaves		$1875 \pm 30 \text{ BP}$	
NBb 47.5	Bb 47.5 Brown moss leaves and stems		2270 ± 30 BP	

ER 7.75	Carex fruits, brown moss stems, Ledum groelandicum leaf	Poz-151143	$104.62 \pm 0.33 \text{ pMC}$
ER 17.25	Carex fruits, Scorpidium scorpioides leaves, Pseudocalliergon trifarium leaves	Poz-151257	900 ± 30 BP
ER 28.25	Carex fruits, brown moss stems	Poz-151256	$1565 \pm 30 \; BP$
ER 36.75	Carex fruits, Scorpidium scorpioides leaves, Pseudocalliergon trifarium leaves	Poz-151258	$2315 \pm 30~\mathrm{BP}$
ER 42.5	Carex fruits x4, brown moss leaves and stems	Poz-109881	$2955 \pm 30 \; BP$
SG 6.25	Scorpidium scorpioides stems with leaves	Poz-151142	$120.77 \pm 0.35 \text{ pMC}$
SG 16.75	Carex fruits and brown moss stems	Poz-151139	$305 \pm 30 \text{ BP}$
SG 26.75	Carex fruits , Betula nana fruits, Scorpidium scorpioides leaves	Poz-151140	$570 \pm 30 \text{ BP}$
SG 36.75	Carex fruits, Scorpidium scorpioides leaves	Poz-151141	$1010 \pm 40 \; BP$
SG 48-49	Carex fruits and stem	Poz-108707	$1680 \pm 35 \text{ BP}$
RH 8.75	Scorpidium stems, Betula nana leaves	Poz-135148	$122.89 \pm 0.32 \text{ pMC}$
RH 17.25	Carex fruits, Carex basal stems	Poz-135149	$655 \pm 30 \text{ BP}$
RH 23.25	Carex fruits, brown moss leaves	Poz-135192	$1460 \pm 30 \text{ BP}$
RH 28.25	wood pieces, brown moss stem	Poz-135193	$1705 \pm 30~\mathrm{BP}$
RH 35-36	wood pieces	Poz-109880	$5000 \pm 40 \; BP$
DL 5	Brown moss	DeA-37949	Modern; post 1950
DL 25	Brown moss and sedge	DeA-37950	1691 ± 21 BP

Table B1b. ²¹⁰ Pb dates at GaI and GaII (for details see Gałka et al., 2023).

Depth (cm)	GaI Age (A.D.)	GaI Error T (1 _o)	GaII Age (A.D.)	GaII Error T (1σ)
0.5	2015.20	0.02	2015.46	030\$5
1.5	2014.0	0.1	2015.21	0.01
2.5	2012.1	0.1	2014.72	0.02
3.5	2010.4	0.1	2014.12	0.03
4.5	2008.7	0.2	2013.35	0.04
5.5	2006.4	0.2	2012.42	0.05
6.5	2002.8	0.3	2011.5	0.1
7.5	1998.9	0.4	2009.9	0.1
8.5	1996.6	0.4	2007.9	300
9.5	1995.0	0.5	2005.2	0.1
10.5	1990.5	0.6	2001.8	0.1
11.5	1986.4	0.7	1997.5	0.2
12.5	1985.4	0.7	1992.6	0.2
13.5	1984.4	0.8	1988.9	0.2
14.5	1983.2	0.8	1985.6	0.3
15.5	1979.2	0.9	1982.6	0.3
16.5	1975	1	1979.8	03.8) 5
17.5	1972	1	1976.8	0.3
18.5	1968	1	1974.0	0.3
19.5	1964	1	1971.4	0.3
20.5	1960	1	1968.1	0.4
21.5	1956	2	1964.1	0.4
22.5	1952	2	1959.3	0.5
23.5	1949	2	1953.9	0.5
24.5	1946	2	1948.1	460
25.5	-	-	1944.0	0.7
26.5	-	-	1941.8	0.7

Fig. B1 Age depth model at TFSI and TFS II (Fig. B1a); GaI and GaII SG (Fig. B1b); NBb and ER (Fig. B1c); RH (Fig. B1d), SG (Fig. B1e) and DL (Fig. B1f). The Y axis represents the depth (cm); the code and position of each radiocarbon measurement are shown inside the plot. The light, dark blue and green shaded areas represent uncertainty ranges in the age-depth model. The black or red histogram shows the possible age of each measured sample. Orage circles indicate ²¹⁰Pb measurements.

410 **Figure B1a**. Age depth model at TFSI and TFS II (Gałka et al., 2018). The light, dark blue and green shaded areas represent uncertainty ranges in the age-depth model.

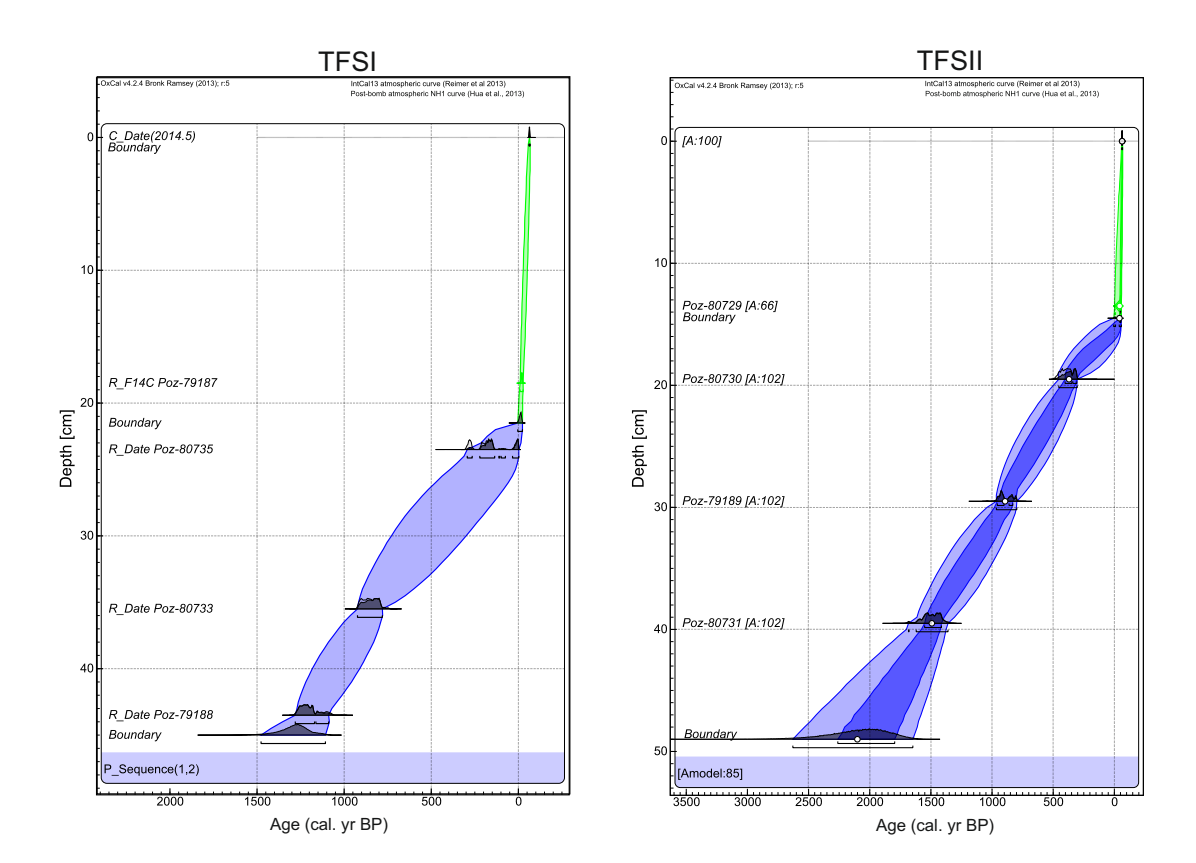
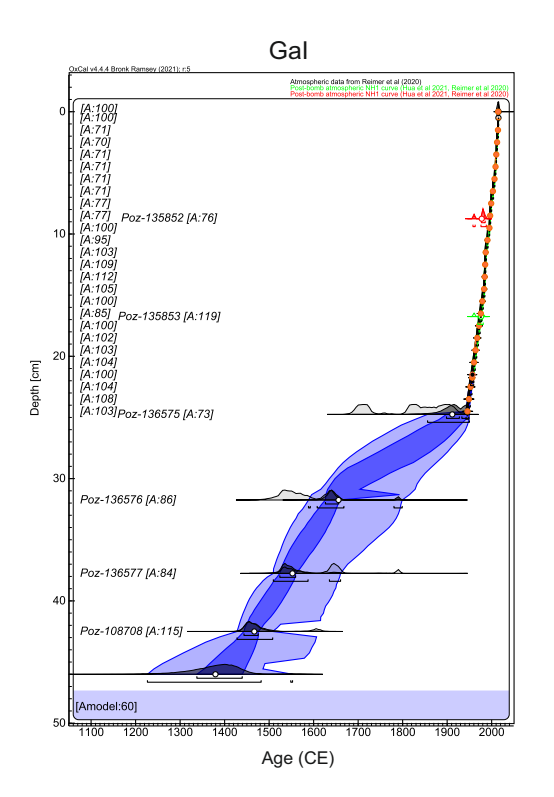


Fig. B1b Age depth model at GaI and GaII (Gałka et al., 2023). The light, dark blue and green shaded areas represent uncertainty ranges in the age-depth model. Orage circles indicate ²¹⁰Pb measurements.



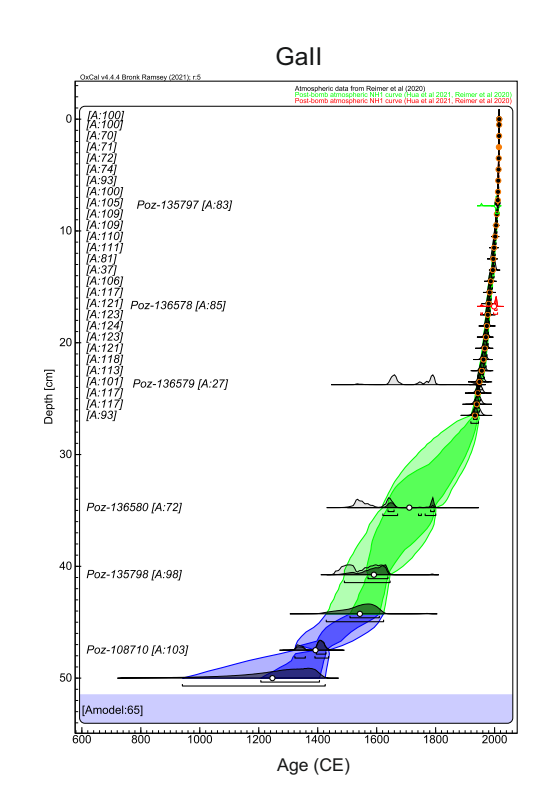


Fig. B1c Age depth model at NBb and ER (Gałka et al., 2025). The light and dark blue shaded areas represent uncertainty ranges in the age-depth model.

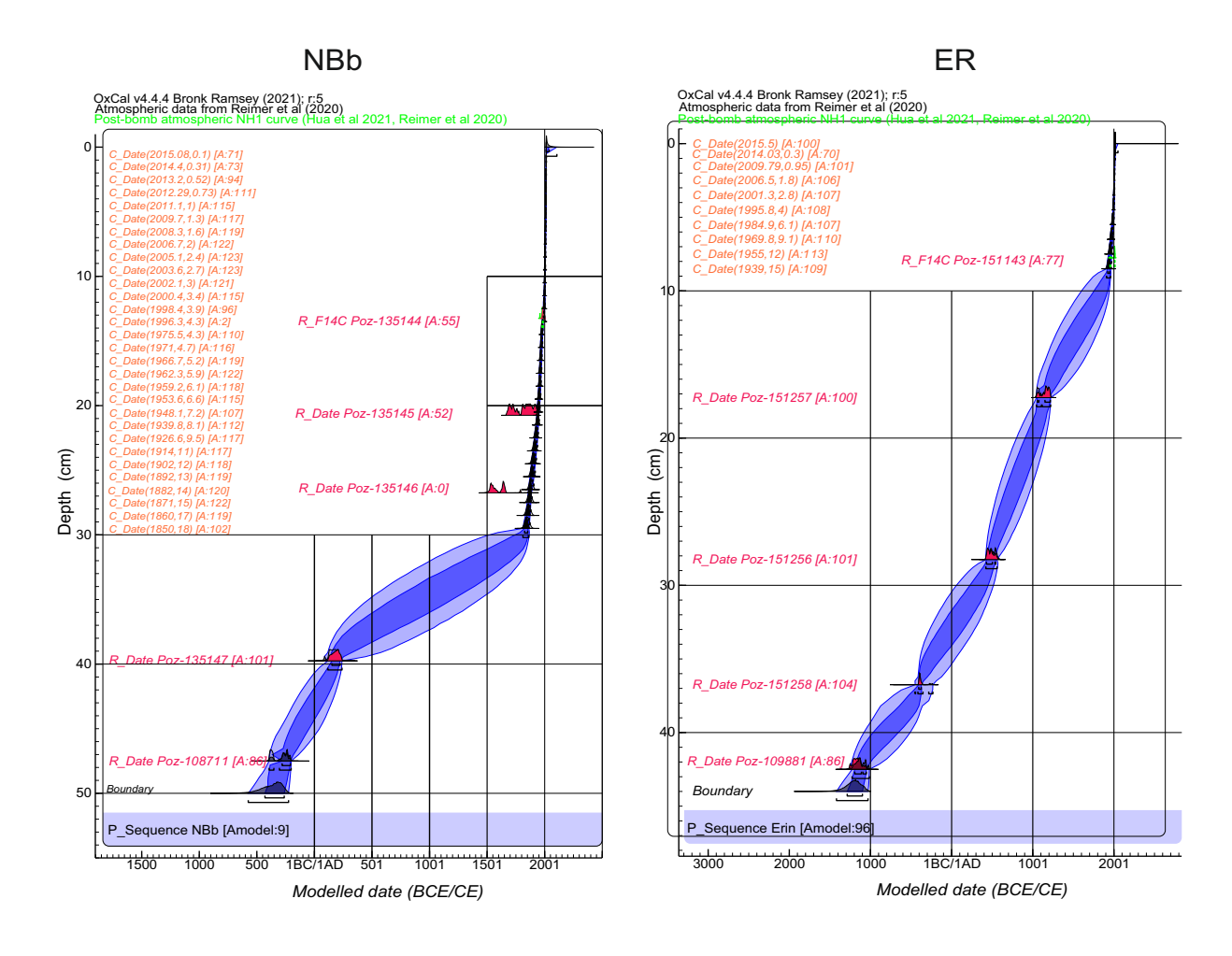


Fig. B1d Age depth model at RH.

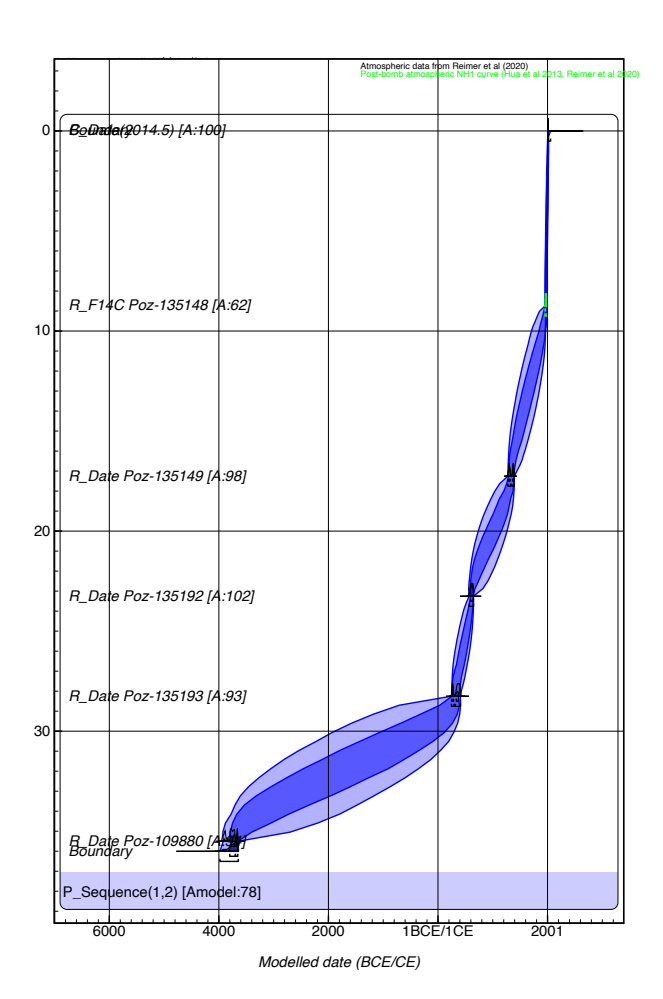


Fig. B1e Age depth model at SG.

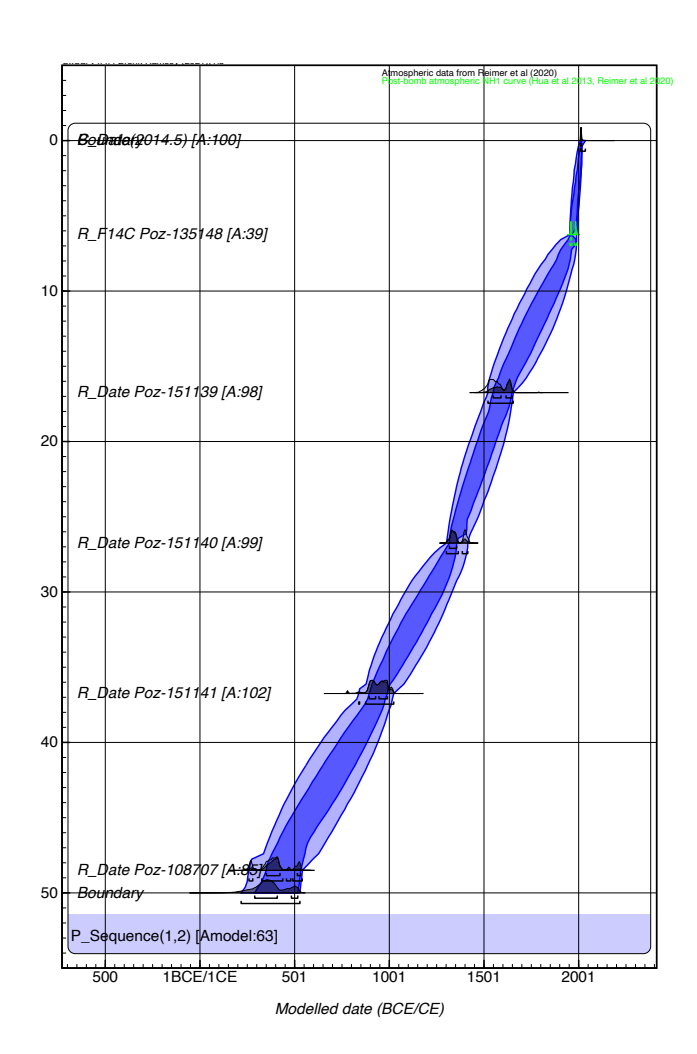
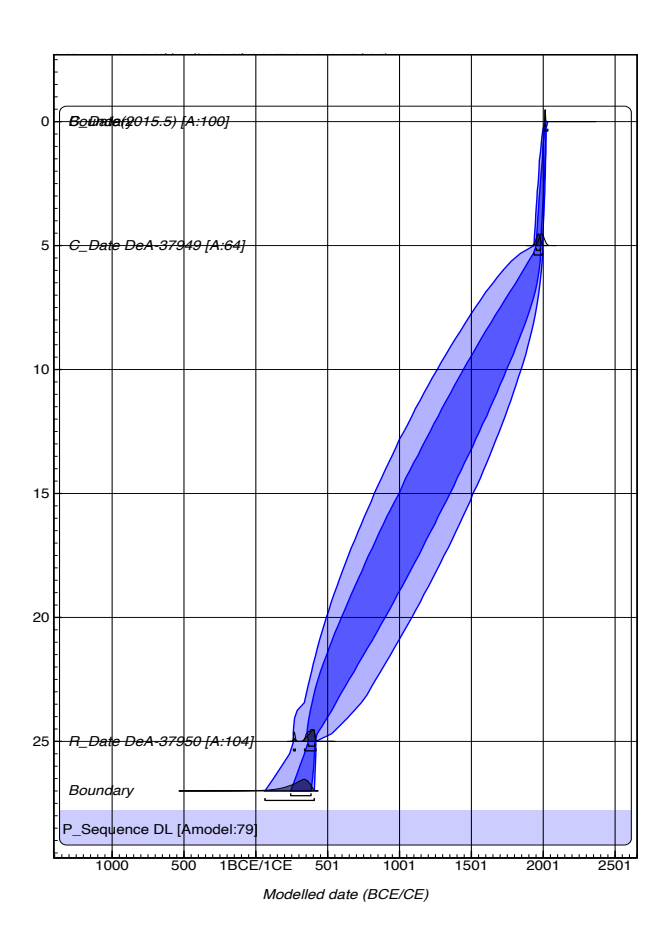
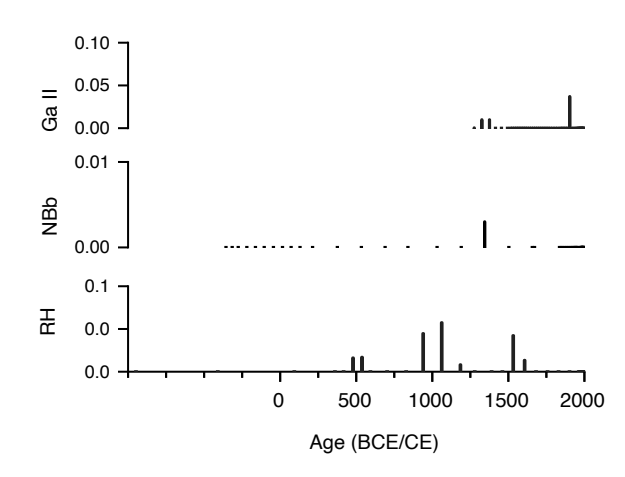


Fig. B1f Age depth model at DL.



Appendix Figure C1. Charcoal influx (#/cm $^{-2}$ yr $^{-1}$) of particles $> 500~\mu m$ in the sequences with available counts size



500 References

- Adolf, C., Wunderle, S., Colombaroli, D., Weber, H., Gobet, E., Heiri, O., van Leeuwen, J. F. N., Bigler, C., Connor, S. E., Gałka, M., La Mantia, T., and Tinner, W.: The sedimentary and remote sensing reflection of biomass burning in Europe, *Glob. Ecol. Biogeogr.*, 27, 199–212, https://doi.org/10.1111/geb.12682, 2018.
- Archibald, S., Lehmann, C. E. R., Gómez-Dans, J. L., and Bradstock, R. A.: Defining pyromes and global syndromes of fire regimes, *Proc. Natl. Acad. Sci. USA*, 110, 6442–6447, https://doi.org/10.1073/pnas.1211466110, 2013.
 - Barhoumi, C., Peyron, O., Joannin, S., Subetto, D., Kryshen, A., Drobyshev, I., Girardin, M. P., Brossier, B., Paradis, L., Pastor, T., and Alleaume, S.: Gradually increasing forest fire activity during the Holocene in the northern Ural region (Komi Republic, Russia), *The Holocene*, **29**, 906–920, https://doi.org/10.1177/0959683619865593, 2019.
- Blarquez, O., Vannière, B., Marlon, J. R., Daniau, A.-L., Power, M. J., Brewer, S., and Bartlein, P. J.: Paleofire An R package to analyse sedimentary charcoal records from the Global Charcoal Database to reconstruct past biomass burning, *Comput. Geosci.*, 72, 255–261, https://doi.org/10.1016/j.cageo.2014.07.020, 2014.
 - Chipman, M. L., Hudspith, V., Higuera, P. E., Duffy, P. A., Kelly, R., Oswald, W. W., and Hu, F. S.: Spatiotemporal patterns of tundra fires: Late-Quaternary charcoal records from Alaska, *Biogeosciences*, 12, 4017–4027, https://doi.org/10.5194/bg-12-4017-2015, 2015.
- Cleary, K. G., Xia, Z., and Yu, Z.: The Growth and Carbon Sink of Tundra Peat Patches in Arctic Alaska, *J. Geophys. Res. Biogeosci.*, 129, e2023JG007890, https://doi.org/10.1029/2023JG007890, 2024.
 - Conedera, M., Tinner, W., Neff, C., Meurer, M., Dickens, A. F., and Krebs, P.: Reconstructing past fire regimes: methods, applications, and relevance to fire management and conservation, *Quaternary Science Reviews*, **28**, 555–576, https://doi.org/10.1016/j.quascirev.2008.11.005, 2009.

- 520 Cox, C. J., Stone, R. S., Douglas, D. C., Stanitski, D. M., Divoky, G. J., Dutton, G. S., Sweeney, C., George, J. C., and Longenecker, D. U.: Drivers and environmental responses to the changing annual snow cycle of northern Alaska, *Bull. Am. Meteorol. Soc.*, 98, 2559–2577, https://doi.org/10.1175/BAMS-D-16-0201.1, 2017.
 - de Groot, W. J., and Wein, R. W.: *Betula glandulosa* Michx. response to burning and postfire growth temperature and implications of climate change, *Int. J. Wildland Fire*, 9, 51–64, https://doi.org/10.1071/WF03048, 1999.
- de Groot, W. J., Cantin, A. S., Flannigan, M. D., Soja, A. J., Gowman, L. M., and Newbery, A.: A comparison of Canadian and Russian boreal forest fire regimes, *For. Ecol. Manag.*, 294, 23–34, https://doi.org/10.1016/j.foreco.2012.07.033, 2013.

- Descals, A., Verger, A., Vilar, L., López-García, M. J., Pettinari, M. L., Tansey, K., and Pons, X.: Unprecedented fire activity above the Arctic Circle linked to rising temperatures, *Science*, 378, 532–537, https://doi.org/10.1126/science.abn9768, 2022.
- Feurdean, A.: Experimental production of charcoal morphologies to discriminate fuel source and fire type: an example from Siberian taiga, *Biogeosciences*, 18, 3805–3821, https://doi.org/10.5194/bg-18-3805-2021, 2021.
- Feurdean, A., Florescu, G., Tanţău, I., Vannière, B., Diaconu, A. C., Pfeiffer, M., Warren, D., Hutchinson, S. M., Gorina, N., Gałka, M., and Kirpotin, S.: Recent fire regime in the southern boreal forests of western Siberia is unprecedented in the last five millennia, *Quaternary Science Reviews*, **244**, 106495, https://doi.org/10.1016/j.quascirev.2020.106495, 2020.
- Feurdean, A., Diaconu, A. C., Pfeiffer, M., Gałka, M., Hutchinson, S. M., Butiseaca, G., Gorina, N., Tonkov, S., Niamir, A., Tantau, I., and Kirpotin, S.: Holocene wildfire regimes in forested peatlands in western Siberia: Interaction between peatland moisture conditions and the composition of plant functional types, *Clim. Past*, 18, 1255–1272, https://doi.org/10.5194/cp-18-1255-2022, 2022.
- 540 Feurdean, A., Veski, S., Florescu, G., Vannière, B., Pfeiffer, M., O'Hara, R. B., Stivrins, N., Amon, L., Heinsalu, A., Vassiljev, J., and Hickler, T.: Broadleaf deciduous forest counterbalanced the direct effect of climate on Holocene fire regime in hemiboreal/boreal region (NE Europe), *Quat. Sci. Rev.*, 169, 378–390, https://doi.org/10.1016/j.quascirev.2017.05.024, 2017.
- Frank-DePue, L. and Chipman, M. L.: Late Holocene tundra fires and linkages to climate and vegetation in Northern Alaska,

 Arctic Science, 11, 1–14, https://doi.org/10.1139/as-2025-0009, 2025.
 - Gałka, M., Swindles, G. T., Szal, M., Fulweber, R., and Feurdean, A.: Response of plant communities to climate change during the late Holocene: palaeoecological insights from peatlands in the Alaskan Arctic, *Ecol. Indic.*, 85, 525–536, https://doi.org/10.1016/j.ecolind.2017.10.062, 2018.
- Gałka, M., Diaconu, A. C., Cwanek, A., Baranov, V. A., Feurdean, A., Loisel, J., Novenko, E. Y., and De Klerk, P.: Climate-induced hydrological fluctuations shape Arctic Alaskan peatland plant communities, *Sci. Total Environ.*, 905, 167381, https://doi.org/10.1016/j.scitotenv.2023.167381, 2023.
 - Hamilton, T. D.: Late Cenozoic glaciation of the central Brooks Range, in: *Glaciation in Alaska: The Geologic Record*, edited by: Hamilton, T. D., Reed, K. M., and Thorson, R. M., Alaska Geological Society, Fairbanks, AK, 9–49, 1986.

- Higuera, P. E., Sprugel, D. G., and Brubaker, L. B.: Reconstructing fire regimes with charcoal from small-hollow sediments: a calibration with tree-ring records of fire, *Holocene*, 15, 238–251, https://doi.org/10.1191/0959683605hl789rp, 2005.
 - Higuera, P. E., Peters, M. E., Brubaker, L. B., and Gavin, D. G.: Understanding the origin and analysis of sediment-charcoal records with a simulation model, *Quat. Sci. Rev.*, 26, 1790–1809, https://doi.org/10.1016/j.quascirev.2007.03.010, 2007.
 - Higuera, P. E., Brubaker, L. B., Anderson, P. M., Brown, T. A., Kennedy, A. T., and Hu, F. S.: Frequent fires in ancient shrub tundra: implications of paleorecords for arctic environmental change, *PLoS ONE*, 3, e1744, https://doi.org/10.1371/journal.pone.0001744, 2008.

- Higuera, P. E., Chipman, M. L., Barnes, J. L., Urban, M. A., and Hu, F. S.: Variability of tundra fire regimes in Arctic Alaska: millennial-scale patterns and ecological implications, *Ecol. Appl.*, 21, 3211–3226, https://doi.org/10.1890/11-0387.1, 2011.
- Hoecker, T. K., Higuera, P. E., Kelly, R., and Hu, F. S.: Arctic and boreal paleofire records reveal drivers of fire activity and departures from Holocene variability, *Ecology*, 101, e03096, https://doi.org/10.1002/ecy.3096, 2020.
 - Hu, F. S., Higuera, P. E., Walsh, J. E., Chapman, W. L., Duffy, P. A., Brubaker, L. B., and Chipman, M. L.: Tundra burning in Alaska: Linkages to climatic change and sea ice retreat, *J. Geophys. Res. Biogeosci.*, 115, G04002, https://doi.org/10.1029/2009JG001270, 2010.
- Hu, F. S., Higuera, P. E., Duffy, P. A., Chipman, M. L., Rocha, A. V., Young, A. M., Kelly, R., and Dietze, M. C.: Arctic tundra fires: Natural variability and responses to climate change, *Front. Ecol. Environ.*, 13, 369–377, https://doi.org/10.1890/150063, 2015.
 - Jones, B. M., Breen, A. L., Gaglioti, B. V., Mann, D. H., Rocha, A. V., Grosse, G., Arp, C. D., Kunz, M. L., and Walker, D. A.: Identification of unrecognized tundra fire events on the North Slope of Alaska, *J. Geophys. Res. Biogeosci.*, 118, 1334–1344, https://doi.org/10.1002/jgrg.20113, 2013.
- Kettridge, N., Turetsky, M., Sherwood, J. H., Thompson, D. K., Miller, C. A., Benscoter, B. W., Flannigan, M. D., Wotton, B. M., and Waddington, J. M.: Moderate drop in water table increases peatland vulnerability to post-fire regime shift, *Sci. Rep.*, 5, 8063, https://doi.org/10.1038/srep08063, 2015.
 - Kuosmanen, N., Väliranta, M., Piilo, S., Tuittila, E.-S., Oksanen, P., and Wallenius, T.: Repeated fires in forested peatlands in sporadic permafrost zone in Western Canada, *Environmental Research Letters*, **18**, 094051, https://doi.org/10.1088/1748-9326/ace7f3, 2023.
 - Loisel, J., Gallego-Sala, A. V., Amesbury, M. J., Magnan, G., Anshari, G., Beilman, D. W., Benavides, J. C., Blewett, J., Camill, P., Charman, D. J., Chawchai, S., et al.: Expert assessment of future vulnerability of the global peatland carbon sink, *Nat. Clim. Change*, 11, 70–77, https://doi.org/10.1038/s41558-020-00944-0, 2021.
- Magnan, G. M., Lavoie, M., and Payette, S.: Impact of fire on long-term vegetation dynamics of ombrotrophic peatlands in northwestern Quebec, Canada, *Quat. Res.*, 77, 110–121, https://doi.org/10.1016/j.yqres.2011.10.006, 2012.
 - Miller, E. A., Jones, B. M., Baughman, C. A., Jandt, R. R., Jenkins, J. L., and Yokel, D. A.: Unrecorded tundra fires of the Arctic Slope, Alaska, USA, *Fire*, 6, 101, https://doi.org/10.3390/fire6030101, 2023.

- Pereboom, E. M., Vachula, R. S., Huang, Y., and Russell, J.: The morphology of experimentally produced charcoal distinguishes fuel types in the Arctic tundra, Holocene, 7, 1–6, https://doi.org/10.1177/0959683620908629, 2020.
- Remy, C. C., Fouquemberg, C., Asselin, H., Andrieux, B., Magnan, G., Brossier, B., Grondin, P., Bergeron, Y., Talon, B., Girardin, M. P., and Blarquez, O.: Guidelines for the use and interpretation of palaeofire reconstructions based on various archives and proxies, *Quaternary Science Reviews*, **193**, 312–322, https://doi.org/10.1016/j.quascirev.2018.06.010, 2018.
 - Reimer, P. J., Bard, E., Bayliss, A., Beck, J. W., Blackwell, P. G., Ramsey, C. B., Buck, C. E., Cheng, H., Edwards, R. L., Friedrich, M., Grootes, P. M., Guilderson, T. P., Haflidason, H., Hajdas, I., Hatté, C., Heaton, T. J., Hoffmann, D. L.,
- Hogg, A. G., Hughen, K. A., Kaiser, K. F., Kromer, B., Manning, S. W., Niu, M., Reimer, R. W., Richards, D. A., Scott, E. M., Southern, J. R., Staff, R. A., Turney, C. S. M., and van der Plicht, J.: IntCal13 and Marine13 radiocarbon age calibration curves 0–50,000 years cal BP, *Radiocarbon*, 55, 1869–1887, https://doi.org/10.2458/azu_js_rc.55.16947, 2013.
- Reimer, P. J., Austin, W. E. N., Bard, E., Bayliss, A., Blackwell, P. G., Bronk Ramsey, C., Butzin, M., Cheng, H., Edwards,
 R. L., Friedrich, M., Grootes, P. M., Guilderson, T. P., Hajdas, I., Heaton, T. J., Hogg, A. G., Hughen, K. A., Kromer, B., Manning, S. W., Muscheler, R., Palmer, J. G., Pearson, C., van der Plicht, J., Reimer, R. W., Richards, D. A., Scott, E. M., Southon, J. R., Turney, C. S. M., Wacker, L., Adolphi, F., Büntgen, U., Capano, M., Fahrni, S. M., Friedrich, R., Köhler, P., Kudsk, S., Miyake, F., Olsen, J., Reinig, F., Sakamoto, M., Sookdeo, A., and Talamo, S.: The IntCal20 Northern Hemisphere radiocarbon age calibration curve (0–55 cal ka BP), *Radiocarbon*, 62, 725–757, https://doi.org/10.1017/RDC.2020.41
 - Raynolds, M.K., Walker, D.A., Maier, H.A.: Plant community-level mapping of arctic Alaska based on the Circumpolar Arctic Vegetation Map. Phytocoenologia. 35(4):821-848. http://doi.org/10.1127/0340-269X/2005/0035-0821, 2005.
 - Sayedi, S. S., Abbott, B. W., Vannière, B., Leys, B., Colombaroli, D., Gil Romera, G., Słowiński, M., Aleman, J. C., Blarquez, O., Feurdean, A., and Brown, K.: Assessing changes in global fire regimes, *Fire Ecol.*, 20, 1–22, https://doi.org/10.1186/s42408-023-00237-9, 2024.

- Scholten, R. C., Jandt, R., Miller, E. A., Rogers, B. M., and Veraverbeke, S.: Overwintering fires in boreal forests, *Nature*, 593, 399–404, https://doi.org/10.1038/s41586-021-03437, 2021.
- Scholten, R. C., Veraverbeke, S., Chen, Y., et al.: Spatial variability in Arctic-boreal fire regimes influenced by environmental and human factors, *Nat. Geosci.*, 17, 866–873, https://doi.org/10.1038/s41561-024-01505-2, 2024.
- Sim, T. G., Swindles, G. T., Morris, P. J., Baird, A. J., Gallego-Sala, A. V., Wang, Y., Blaauw, M., Camill, P., Garneau, M., Hardiman, M., and Loisel, J.: Regional variability in peatland burning at mid- to high-latitudes during the Holocene, *Quat. Sci. Rev.*, 305, 108020, https://doi.org/10.1016/j.quascirev.2023.108020, 2023.
- Swindles, G. T., Morris, P. J., Mullan, D. J., Payne, R. J., Roland, T. P., Amesbury, M. J., Lamentowicz, M., Turner, T. E., Gallego-Sala, A., Sim, T., and Barr, I. D.: Widespread drying of European peatlands in recent centuries, *Nat. Geosci.*, 12, 922–928, https://doi.org/10.1038/s41561-019-0462-z, 2019.

- Taylor, L. S., Swindles, G. T., Morris, P. J., et al.: Evidence for ecosystem state shifts in Alaskan continuous permafrost peatlands in response to recent warming, *Quat. Sci. Rev.*, 207, 134–144, https://doi.org/10.1016/j.quascirev.2019.02.001, 2019.
- Turetsky, M., Benscoter, B., Page, S., Rein, G., van der Werf, G. R., and Watts, A.: Global vulnerability of peatlands to fire and carbon loss, *Nat. Geosci.*, 8, 11–14, https://doi.org/10.1038/ngeo2325, 2015.
 - Vachula RS, Sae-Lim J, Russell JM. Sedimentary charcoal proxy records of fire in Alaskan tundra ecosystems. Palaeogeography, Palaeoclimatology, Palaeoecology. 1;541:109564.
 - Vachula, R. S., Sae-Lim, J., and Li, R.: A critical appraisal of charcoal morphometry as a paleofire fuel type proxy, *Quat. Sci. Rev.*, 262, 106979, https://doi.org/10.1016/j.palaeo.2019.109564, 2021.
- Vachula, R. S. and Rehn, E.: Modeled dispersal patterns for wood and grass charcoal are different: implications for paleofire reconstruction, *Holocene*, 33, 159–166, https://doi.org/10.1177/09596836221131708, 2023.
 - Walker, M. D., Walker, D. A., and Auerbach, N. A.: Plant communities of a tussock tundra landscape in the Brooks Range Foothills, Alaska, *J. Veg. Sci.*, 5, 843–866, https://doi.org/10.2307/3236198, 1994.
 - Walker, D. A., Raynolds, M. K., Daniëls, F. J. A., et al.: The Circumpolar Arctic vegetation map, *J. Veg. Sci.*, 16, 267–282, https://doi.org/10.1111/j.1654-1103.2005.tb02365.x, 2005.

- Whitman, E., Parisien, M.-A., Thompson, D. K., and Flannigan, M. D.: Topoedaphic and forest controls on post-fire vegetation assemblies are modified by fire history and burn severity in the northwestern Canadian boreal forest, *Forests*, 9, 151, https://doi.org/10.3390/f9030151, 2018.
- Whitman, E., Parisien, M.-A., Thompson, D. K., and Flannigan, M. D.: Short-interval wildfire and drought overwhelm boreal forest resilience, *Sci. Rep.*, 9, 16519, https://doi.org/10.1038/s41598-019-55036-7, 2019.
 - Stivrins, N., Aakala, T., Ilvonen, L., Pasanen, L., Kuuluvainen, T., Vasander, H., Gałka, M., Disbrey, H. R., Liepins, J., Holmström, L., and Seppä, H.: Integrating fire-scar, charcoal and fungal spore data to study fire events in the boreal forest of northern Europe, *The Holocene*, **29**, 1480–1490, https://doi.org/10.1177/0959683619854524, 2019.
- Zhang, H., Väliranta, M., Swindles, G. T., et al.: Recent climate change has driven divergent hydrological shifts in high-latitude peatlands, *Nat. Commun.*, 13, 4959, https://doi.org/10.1038/s41467-022-32711-4, 2

Figure legends and embedded figures

Figure 1a,b. Location of the study area in northern Alaska. Charcoal sampling sites numbered 1 to 9 are situated along the Dalton Highway, extending from the northern slope of the Brooks Range Mountains to the Arctic Ocean. Site names and coordinates are listed in Table 1. Figure 1a depicts large fires as polygons and their respective time of occurrence. Figure 1b represents small fires as points, with colour coding of each fire point indicating the decade in which the fire occurred, while the numbers refer to their specific locations (for fire names, coordinates, size, and distance from the Dalton Highway and sampling sites see S1).

Figure 1a.

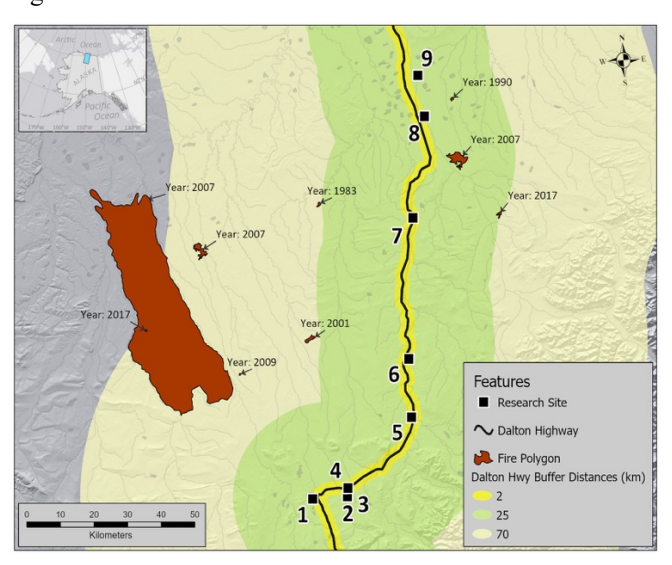


Figure1b

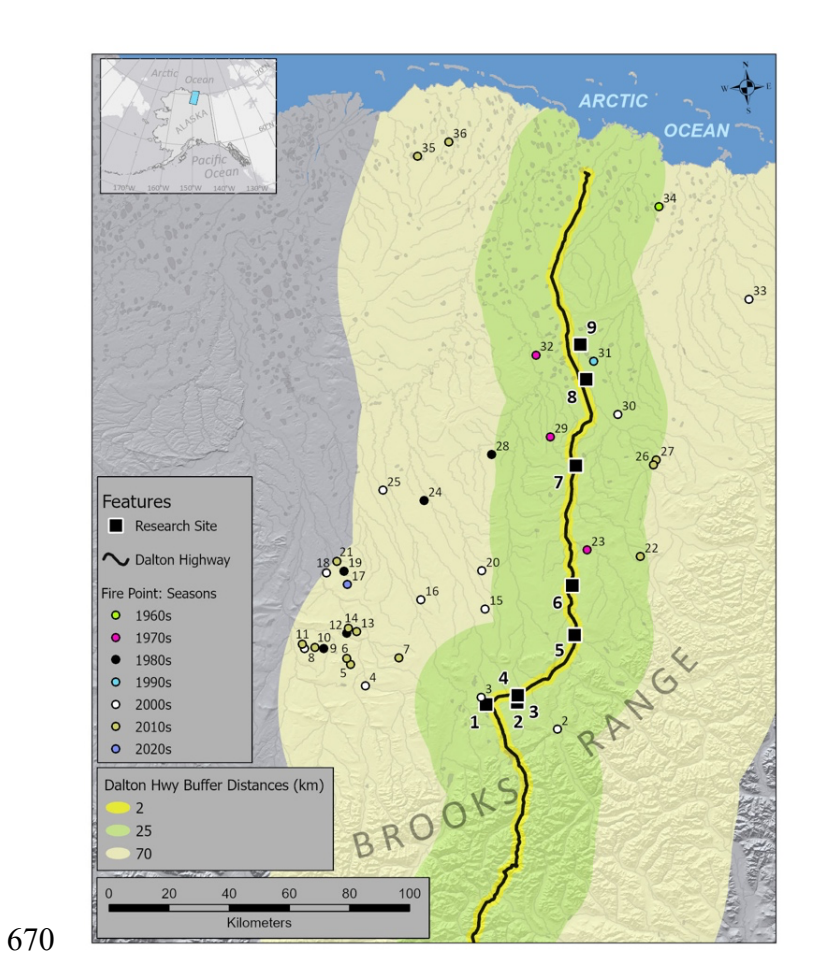
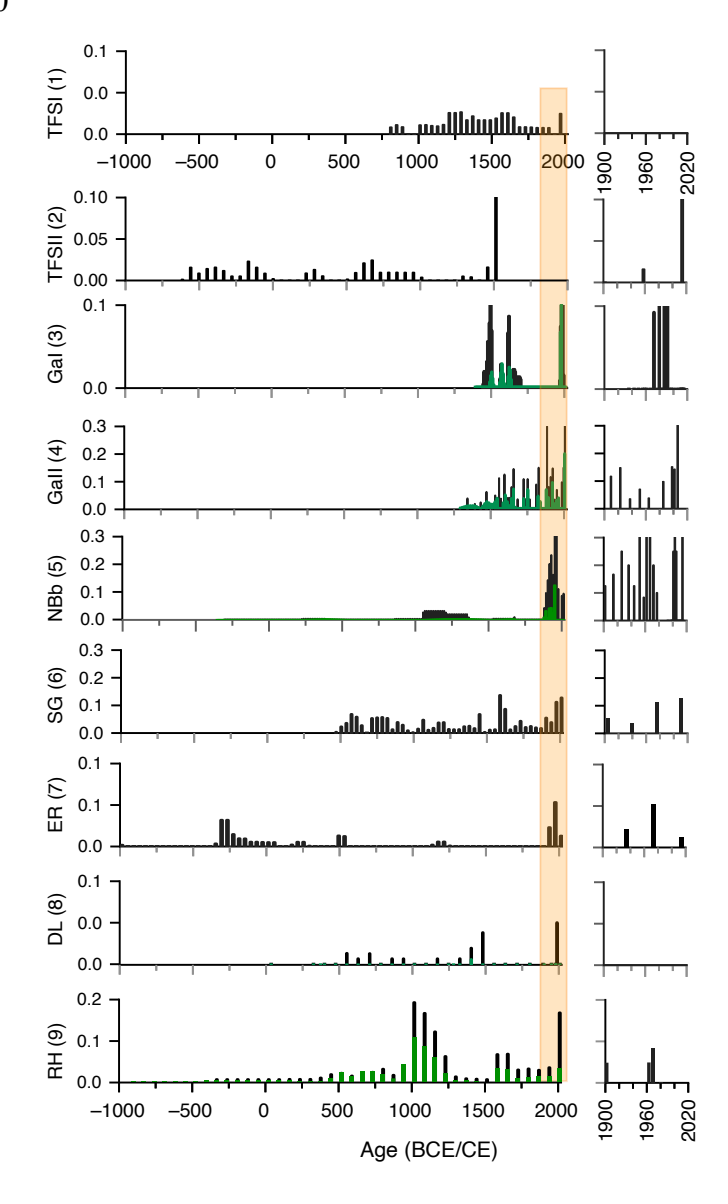


Figure 2. Total interpolated charcoal accumulation rates (black bars) and separated on woody charcoal morphologies (green bars; particles cm⁻² yr⁻¹) at nine sites along the Dalton Highway. The numbers in brackets indicate the site numbers as marked in Fig. 1. At sites with identified woody morphologies, the difference between the total charcoal and the woody morphology represents the morphologies formed by herbs (grass leaves, stems of forbs, and grasses) and broadleaves. On the right-hand side are trends in charcoal charcoal accumulation rates over the last century. The orange rectangle highlights the period of marked increase in total charcoal influx. BCE=before Common Era; CE Common Era.



Figures 3. a) Composite record of biomass burning (n=9) based on Z-score charcoal accumulation rates, where positive/negative Z-score values represent greater-than-mean/lower-than-mean charcoal amount, over the base period, interpreted as high/lower values in biomass burning. b) Composite record (n=5) of the abundance of shrubs determined from pollen and plant macrofossils, where pollen and root shrub biomass are represented as %, and above-ground remains (seeds, leaves, fruits) as counts (c). Composite record of peatland hydrology (n=5) from testate amoeba, where positive/negative Z-score values represent higher (shallow) /lower (deep) than the mean water level. Grey shadows represent confidence intervals. The inserts represent trends over the last two centuries.

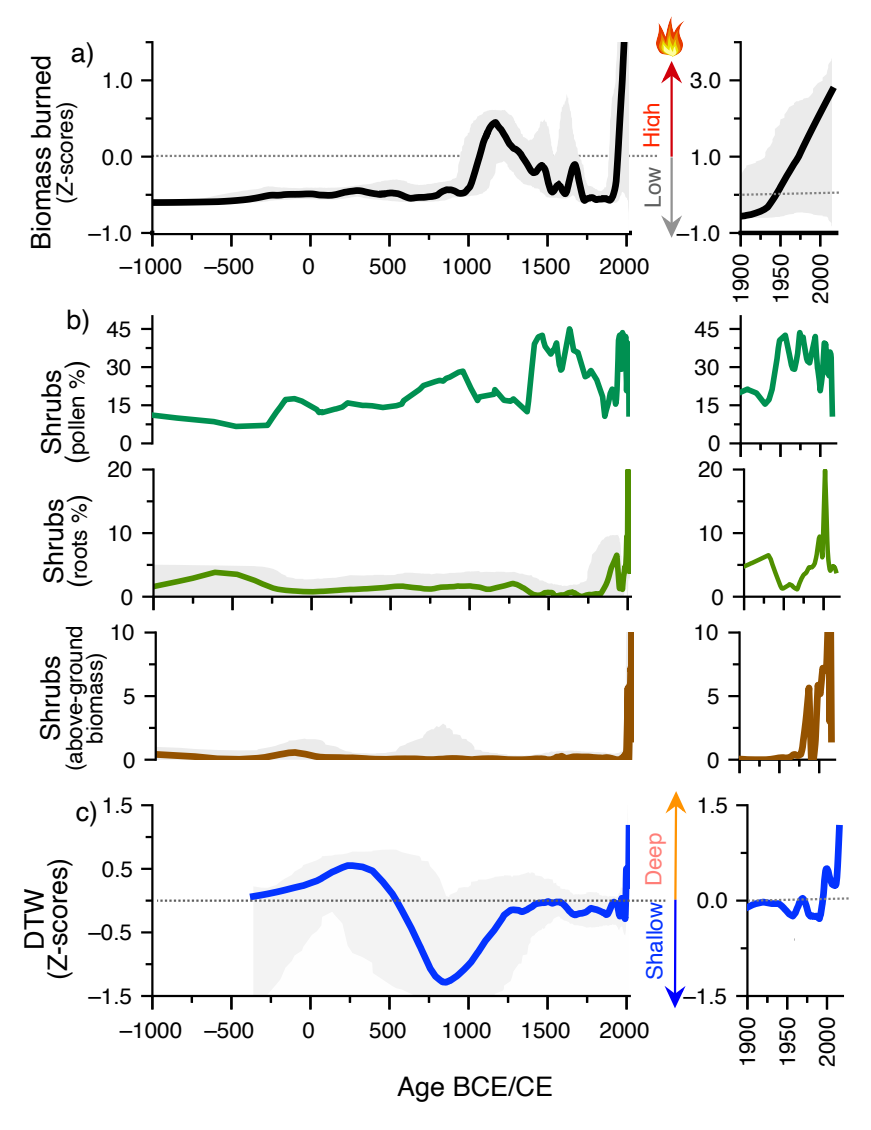
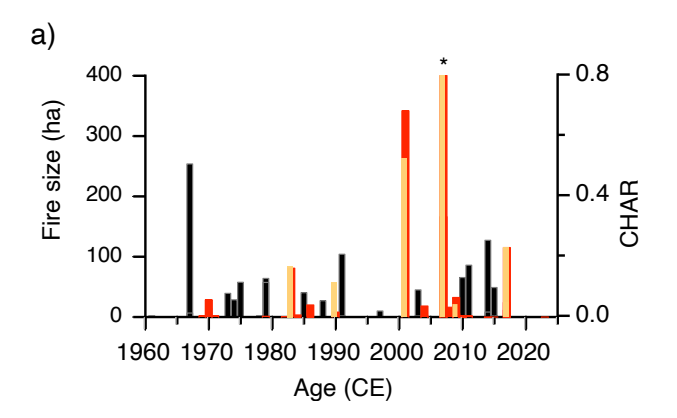


Figure 4. a) Comparison of fire frequency and size (ha) represented as fire points (red bars) and fire polygons (orange bars)
from satellite imagery with interpolated charcoal influx (black bars; particles cm⁻² yr⁻¹): *Note: The full extent of large fire occurring in 2007 (103896 ha) is not shown to improve visibility of trends in smaller fire events. b) Distance to nearest five fires from each of the sites: I=denote the nearest and V= the furthest from each of the sites.



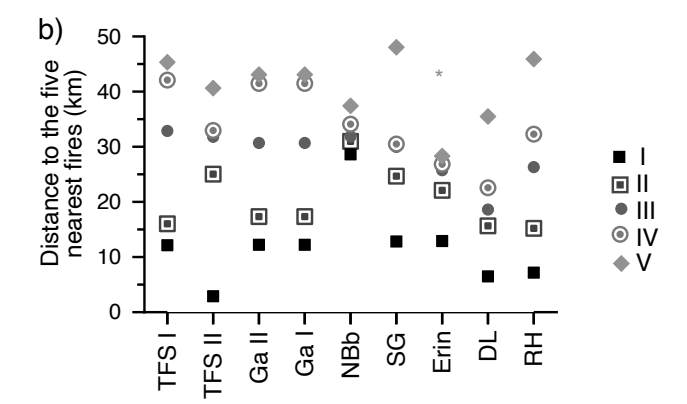


Table 1. Information on site ID, geographic coordinates, elevation, core lengths (in cm and age), the dominant vegetation, and references at the coring points.

	Site	Coordinates	Elev.	Core (cm)	Age range (BCE/CE)	Dominant vegetation Reference	e
730	1. TFS1	68.6239, 149.3458	715	45	2014-688	Sphagnum fuscum, S. capillifolium, Andromenda polifolia, Betula nana	Galka et al., 2018
, 2 0	2. TFS2	68.6239, 149.5978	750	50	2010-118 BCE	S. capillifolium, A. polifolia, Betula nana	Galka et al., 2018
	3. Gal I	68.6453, 149.3375	876	46	2015-1400	Paludellla squarrosa, Carex spp. Andromenda polifolia, Betula nana,	Galka et al., 2023
735	4. Gal II	68.6453, 149.3375	876	50	2015-1300	Dryas octopetala, Salix spp., Rubus chamaemorus, Sphagnum teres, S. warnstorfii	Galka et al., 2023
740	5. NBb	68.8136, 148.8406	461	50	2015-300 BCE	Scorpidium scorpioides, S. cossonii, Carex spp., Sphagnum subfulvum, Betula nana, Dryas octopetala, Salix spp., Rubus chamaemorus	Galka et al., 2025
	6. SG	68.9647, 148.0841	159	50	2010-400	Carex spp., Tomentypnum nitens, Andromeda polifolia, Arctostaphyllos, Dryas octopetala, Salix	This study
745	7. Erin (ER)	69.3233, 148.7208	230	44	2015-1125 BCE	Carex spp., Tomentypnum nitens, Scorpidium cossonii, Betula nana, Dryas octopetala, Salix Rubus chamaemorus spp.	Galka et al., 2025
750	8. DL	69.5811, 148.5765	159	49	2008-3000 BCE	Carex spp., Scorpidium scorpioides, Bryum pseudotriquetrum	This study
, 2 0	9. RH	69.6875, 148.6017	156	36	2011-2600 BCE	Carex spp., Scorpidium revolvens, Dicranum sp., Ledum groelandicum, Salix sp	This study